NeuroImage 63 (2012) 1020–1029

Contents lists available at SciVerse ScienceDirect

NeuroImage

journal homepage: www.elsevier.com/locate/ynimg

Short- and long-term quantitation reproducibility of brain metabolites in the medial wall using proton echo planar spectroscopic imaging

Shang-Yueh Tsai [a,b], Yi-Ru Lin [c], Woan-Chyi Wang [c], David M. Niddam [d,e,f,*]

[a] Graduate Institute of Applied Physics, National Chengchi University, Taipei, Taiwan
[b] Research Center for Mind, Brain and Learning, National Chengchi University, Taipei, Taiwan
[c] Department of Electronic Engineering, National Taiwan University of Science and Technology, Taipei, Taiwan
[d] Brain Research Center, National Yang-Ming University, Taipei, Taiwan
[e] Institute of Brain Science, National Yang-Ming University, Taipei, Taiwan
[f] Laboratory of Integrated Brain Research, Department of Medical Research and Education, Taipei Veterans General Hospital, Taipei, Taiwan

ARTICLE INFO

Article history:
Accepted 18 July 2012
Available online 27 July 2012

Keywords:
Glutamate
Glutamine
Cingulate
TE averaging
Sagittal 2D MRSI
PEPSI

ABSTRACT

Proton echo planar spectroscopic imaging (PEPSI) is a fast magnetic resonance spectroscopic imaging (MRSI) technique that allows mapping spatial metabolite distributions in the brain. Although the medial wall of the cortex is involved in a wide range of pathological conditions, previous MRSI studies have not focused on this region. To decide the magnitude of metabolic changes to be considered significant in this region, the reproducibility of the method needs to be established. The study aims were to establish the short- and long-term reproducibility of metabolites in the right medial wall and to compare regional differences using a constant short-echo time (TE30) and TE averaging (TEavg) optimized to yield glutamatergic information. 2D sagittal PEPSI was implemented at 3 T using a 32 channel head coil. Acquisitions were repeated immediately and after approximately 2 weeks to assess the coefficients of variation (COV). COVs were obtained from eight regions-of-interest (ROIs) of varying size and location. TE30 resulted in better spectral quality and similar or lower quantitation uncertainty for all metabolites except glutamate (Glu). When Glu and glutamine (Gln) were quantified together (Glx) reduced quantitation uncertainty and increased reproducibility was observed for TE30. TEavg resulted in lowered quantitation uncertainty for Glu but in less reliable quantification of several other metabolites. TEavg did not result in a systematically improved short- or long-term reproducibility for Glu. The ROI volume was a major factor influencing reproducibility. For both short- and long-term repetitions, the Glu COVs obtained with TEavg were 5–8% for the large ROIs, 12–17% for the medium sized ROIs and 16–26% for the smaller cingulate ROIs. COVs obtained with TE30 for the less specific Glx were 3–5%, 8–10% and 10–15%. COVs for N-acetyl aspartate, creatine and choline using TE30 with long-term repetition were between 2–10%. Our results show that the cost of more specific glutamatergic information (Glu versus Glx) is the requirement of an increased effect size especially with increasing anatomical specificity. This comes in addition to the loss of sensitivity for other metabolites. Encouraging results were obtained with TE30 compared to other previously reported MRSI studies. The protocols implemented here are reliable and may be used to study disease progression and intervention mechanisms.

Introduction

Magnetic resonance spectroscopy (MRS) is a non-invasive imaging technique that allows quantifying several metabolites at the same time in the human brain. Proton MRS can simultaneously obtain information about a diverse range of functions including neuronal integrity, glial function, bioenergetics, membrane turnover, and glutamatergic and glutaminergic neurotransmission (Soares and Law, 2009). As the major excitatory neurotransmitter in the brain, glutamate (Glu) can provide knowledge about hyper- or hypo-excitation and excitotoxicity associated with, for example, epilepsies and neurodegenerative diseases (Pan et al., 2008; Petroff et al., 2002; Srinivasan et al., 2005). Glutamine (Gln) is also the precursor of Glu and gamma-amino butyric acid and may also be related to the recycling and storage of these neurotransmitters (Hertz, 2004).

Short echo-times (TEs) have been used to detect Glu and Gln in the proton spectrum. However, due to spectral overlap caused by similarities in the chemical structure, the combined concentration of Glu and Gln (Glx) is often quantified. Although higher magnetic field strength offers larger frequency dispersion, it remains challenging to measure Glu and Gln even at 3 T (Mullins et al., 2008). Several methods have been proposed to resolve this issue including a spectral editing method

* Corresponding author at: Brain Research Center, National Yang-Ming University, No. 155, Section 2, Linong Street, Taipei 112, Taiwan. Fax: +886-2-28273123.
E-mail address: niddam@ym.edu.tw (D.M. Niddam).

1053-8119/$ – see front matter © 2012 Elsevier Inc. All rights reserved.
http://dx.doi.org/10.1016/j.neuroimage.2012.07.039

using TE averaging to enhance Glu in the spectrum while suppressing Gln (Hurd et al., 2004; Srinivasan et al., 2006). This method is faster than other editing methods (Srinivasan et al., 2006) but the reliability for successive acquisitions may not necessarily improve compared with constant short-TEs (Gonenc et al., 2010; Mullins et al., 2008).

Most proton MRS studies have employed a single voxel with relatively large dimensions placed at an a priori selected location. With the development of fast MR spectroscopic imaging (MRSI) techniques, such as proton echo planar spectroscopic imaging (PEPSI), it is possible to collect spectral data from multiple regions in relatively short time. Spatial metabolite distributions can be mapped and related directly to the brain anatomy. Similar to other imaging modalities, MRS can measure short-term functional changes in response to external stimuli (Mangia et al., 2007; Mullins et al., 2005) or monitor longitudinal changes related to disease progression and intervention mechanisms (Harris et al., 2008). However, to be able to obtain meaningful results from both types of paradigms, the reproducibility of the method needs to be established since this will decide the magnitude of metabolic changes to be considered significant. Previous MRSI studies found the reproducibility to vary spatially and to depend on the specific metabolite as well as the sample volume (Chard et al., 2002; Gu et al., 2008; Li et al., 2002; Maudsley et al., 2010; Tedeschi et al., 1996). For single voxels and volumes covering lobar regions, variability of the three major metabolites have been reported to be around 6–22% (Chard et al., 2002; Langer et al., 2007; Li et al., 2002) and 3–7% (Maudsley et al., 2010), respectively.

The medial wall of the cortex contains structures of the limbic system and regions involved in top-down modulatory processes. These regions contribute to a wide range of pathological conditions including psychiatric disorders and chronic pain (Apkarian et al., 2011; Bennett, 2011). Previous MRSI studies have not specifically focused on this region and most have acquired slices in the transverse plane. This may not be optimal for coverage of the medial wall which is located in the sagittal plane. The aims of the present study were: (1) to establish the short- and long-term reproducibility of metabolites in the medial wall using 2-dimensional PEPSI acquired in the sagittal plane; (2) to assess the reproducibility in selected regions-of-interests (ROIs) varying in anatomical location and in size; and (3) to compare regional reproducibility of metabolites, in particular Glu, Gln and Glx, using a constant short-TE (TE30) and TE-averaging (TEavg). Short-term reproducibility was measured in the same scan session to mimic the immediate repetition used in functional paradigms in which the participant remains in the scanner. Long-term reproducibility was measured with about 2 week's interval to mimic longitudinal follow-up studies. It accounts for instrumental variation and variations in positioning of the participant in the scanner. The protocols provided the same clinically feasible scan time, i.e. less than 10 min, while maintaining a reasonable signal-to-noise ratio (SNR).

Methods

Subjects

Sixteen normal volunteers (9 females/7 males; mean age ± standard deviation [SD]: 29.9 ± 8.2 years; age range: 21–49 years) participated in this study. All subjects were scanned to evaluate the MRSI reproducibility obtained with the TE30 protocol and the TEavg protocol. Each protocol was repeated twice in the same scan session for the assessment of short-term (within-day) reproducibility without leaving the scanner. Eight subjects returned around two weeks later (interval: 9–22 days; mean ± SD: 14.6 ± 4.2 days) to repeat the same procedure for the assessment of long-term (between-weeks) reproducibility. For psychological assessment, all participants completed the Spielberger State-Trait Anxiety Inventory and the Beck Depression Inventory (Beck et al., 1961) prior to the first scan. Before being included in the study, participants gave their informed consent to the protocol, which was approved by the Institutional Review Board of National Yang-Ming University.

Data acquisition

MRI and MRSI experiments were carried out on a 3 T MR system (Trio, SIEMENS Medical Solutions, Erlangen, Germany) with a 32-channel head coil array. Initially, we acquired a high-resolution 3D MPRAGE (Magnetization Prepared Rapid Acquisition Gradient Echo) anatomical scan (repetition time [TR]/echo time [TE]/flip angle [FA]: 2530 ms/3.03 ms/7°; field of view [FOV]: 224 × 256 × 192; voxel size: 1 × 1 × 1 mm^3) for localization of the right medial wall, as required for subsequent MRSI scans. A high speed MRSI method, PEPSI (Lin et al., 2007; Tsai et al., 2007, 2008), was used for the acquisition of MRSI data. Two-dimensional MRSI data were acquired with an in-plane resolution of 8 × 8 mm with a 256 × 256 mm FOV. A 14-mm thick sagittal plane was selected to cover the medial wall in the right hemisphere. Up to eight slices of outer-volume lipid suppression were applied along the perimeter of the brain to suppress the lipid signal. To reduce the partial volume effect from cerebrospinal fluid, the MRSI plane was placed slightly away from the central line. Experimental parameters for the TE30 protocol were TR = 1.5 s, TE = 30 ms, and number of excitations (NEX) = 8. For the TEavg protocol, 8 echo steps from 35 ms to 185 ms with 20 ms increments were acquired with a TR of 1.5 s to match the scan time of the TE30 protocol. A non-water suppressed (NWS) MRSI scan without pre-saturation of the water signal was acquired using a single average for automatic phase correction and calibration of metabolite concentrations. Field shimming and a NWS scan was performed for each of the TE30 and TEavg acquisitions. The total acquisition time for all PEPSI scans were 36 min. After the PEPSI scans, multi-slice sagittal T1-weighted images were collected using a gradient echo sequence (TR/TE/FA: 250 ms/2.61 ms/70°; FOV: 256 × 256; MAT: 128 × 128; slice thickness: 2 mm). Seven slices were collected yielding a 14 mm volume to cover the same spatial location as the PEPSI scan. These T1 images were used as anatomical reference in the following regional analysis.

Post processing

MRSI data from the different coils and measurements were processed individually. Standard post processing strategies, including spatial and temporal filtering, phase correction and even-odd echo editing, were performed for the PEPSI data as described previously (Lin et al., 2007; Tsai et al., 2007, 2008). The reconstructed spectral width of the PEPSI data after even/odd echo editing was 1086 Hz with 512 complex points yielding a spectral resolution of 2.1 Hz. MRSI data from the different coils were combined after phase correction to avoid possible artifacts caused by partial phase cancelation. Frequency adjustment was applied to the different measurements in the TE30 dataset and the different TEs in the TEavg dataset. Finally, data from the eight measurements with constant TE and step-wise TEs were averaged separately to yield spectra for the two protocols.

Spectra were quantified with LCModel-based spectral fitting in the range from 0.5 to 4 ppm (Provencher, 1993). Basis sets for spectral fitting were generated with the Gamma Visual Analysis tool (Soher et al., 2007). Simulated spectra for 17 metabolites (including macromolecules and lipids) at different TEs were exported and converted into LCModel basis spectra. The basis set for the TEavg protocol was created by averaging the simulated spectra at the different TEs. Metabolite concentrations of N-acetyl aspartate (NAA), total creatine (tCr; including creatine and phosphocreatine), total choline (tCho), myo-inositol (mI), glutamate (Glu), glutamine (Gln), and the combination of glutamate and glutamine (Glx) were obtained using the water-scaling method (Gasparovic et al., 2006). With this method, the metabolite signal is calibrated to that of the water signal without considering relaxation and partial volume effects. Hence, the quantified metabolite concentrations are provided in institutional units (I.U.).

Metabolites were evaluated in eight regions-of-interest (ROIs) and included the cortex of the right medial wall (MW), the cingulate cortex (CC), the anterior CC, the middle CC, the posterior CC, the thalamus, the medial parietal lobe, and the medial occipital lobe. Each ROI was manually selected on the individual T1 images. The MW mask was defined as the largest contour of the tCr metabolite map and excluded spurious spikes at the edge of the cortex. The CC mask was adjusted according to the shape and size of the individual structure (Fig. 1A). The other masks consisted of a fixed square matrix grid. For the anterior CC, the middle CC, the posterior CC, and the thalamus the grid size was 2×2 voxels. For the occipital and parietal lobes the grid sizes were 3×3 voxels and 4×4 voxels, respectively (Fig. 1B). For statistical analysis, the mean and standard deviation of metabolite concentrations inside the ROIs were calculated. In addition, the Cramer–Rao Lower Bound (CRLB), as provided by LCModel, was used as the error metric for metabolite quantification. It is the lowest bound of the standard deviation of the estimated metabolite concentration and is expressed in concentration percentage. The CRLB for each metabolite is commonly used to quantify the goodness-of-fit in LCModel (Provencher, 1993). For the calculation of concentrations we used the following thresholds to reject voxels with unsatisfactory LCModel fit: CRLB > 20% for NAA, tCr and tCho, and CRLB > 50% for mI, Glu, Gln and Glx. Evaluation of the spectral quality was based on the linewidth at full-width at half maximum (FWHM; in parts per million) and the SNR as provided by LCModel.

Statistical analysis

The within-day and between-weeks reproducibility of the TE30 and TEavg protocols were assessed by the coefficient of variation (COV). COVs were calculated as the root mean square of the standard deviation of the two measurements divided by the mean across all subjects. Subjects were excluded from the COV analysis if less than two voxels within the ROI satisfied the CRLB threshold. This typically occurred in regions where field homogeneity adjustments are challenging (prefrontal and inferior areas), in regions with broadened spectral lines leading to unsuccessful spectral fitting (anterior CC and thalamus), and for Gln in the TEavg protocol due to successful suppression. A paired t-test was used to assess spectral quality and Glu and Glx differences in spectral fitting (CRLB) for the two protocols. Inter subject variations were investigated by mean and standard deviation of metabolite concentrations from the first scan of each subject.

Results

According to the psychological assessment of the participants performed before the first scan, anxiety (state: 40.6 ± 6.8; trait: 45.2 ± 7.1) and depression (6.35 ± 4.1) scores were within the normal range suggesting that the study sample was without significant mood disturbance. To evaluate the effects of shimming, regions of signal extinction, and possible spatial distortions, the non-water-suppressed (NWS) signal distribution and spectral quality distributions were inspected (Fig. 2). The outer contour of the water-signal distribution was found to match the anatomical image. NWS signal extinction was not observed in the ventral prefrontal region. However, broadened linewidths and poor SNRs were found in this region as well as in the brain stem and to some extend in the occipital cortex. These effects are most likely due to shimming (field homogeneity) issues and partial volume effects and agree with the variation in the anatomical structure. The SNR map did not reveal a systematic bias toward surface regions, e.g. the thalamic SNR was of similar magnitude as the cingulate SNRs. This suggests that the enhanced coil sensitivity near the brain surface observed with phased array detection may have little influence on our results.

The spectral quality of the water-suppressed proton spectra differed between the two protocols and between anatomical regions. For all ROIs, TE30 resulted in significantly higher SNR ($P<0.001$) even after a Bonferroni adjustment for the number of ROIs tested (8 ROIs, $P<0.00625$) (Table 1). For both protocols, the posterior CC ROI exhibited the highest SNR and the thalamic ROI and the medial-wall ROI exhibited the lowest SNRs. The two protocols resulted in comparable spectral linewidth for all ROIs except the two largest ROIs covering the medial wall and the CC for which smaller FWHMs were found for TEavg. Only the former survived a corrected threshold. Also, for both protocols, wider spectral linewidths were observed for the thalamic, occipital and parietal ROIs. Visual inspection of the spectra (Fig. 3) obtained by the two protocols confirmed a moderate signal loss as well as a flattened baseline for TEavg. In addition, the emergence of the unobstructed glutamate peak at 2.35 ppm and a substantial reduction in the mI peak at around 3.5 ppm were also observed.

Interpolated metabolite maps from the right medial wall and the matched uninterpolated CRLB maps from the first scans are shown in Fig. 4 for a representative subject. For TEavg, the suppression of the Gln peak and the reduction of the mI peak resulted in highly spatial non-uniform concentrations maps and increased CRLBs. Although the mean concentrations differed between the two TE protocols they exhibited similar regional dependencies. In general, for all metabolites but tCho, the highest concentrations were found in the occipital and

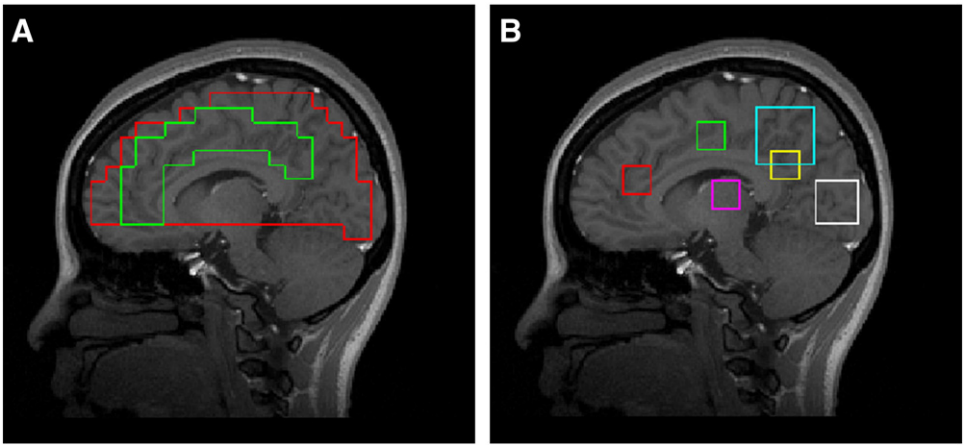

Fig. 1. Regions-of-interest (ROIs) for a representative subject. (A) ROIs adjusted according to the shape and size of the individual brain structure included the entire cortex of the right medial wall (red) and the cingulate cortex (CC; green). (B) Smaller fixed-size ROIs were located in the anterior CC (red), the middle CC (green), the posterior CC (yellow), the thalamus (pink), the medial parietal lobe (blue), and the medial occipital lobe (white). ROI locations were manually selected on the individual T1 images.

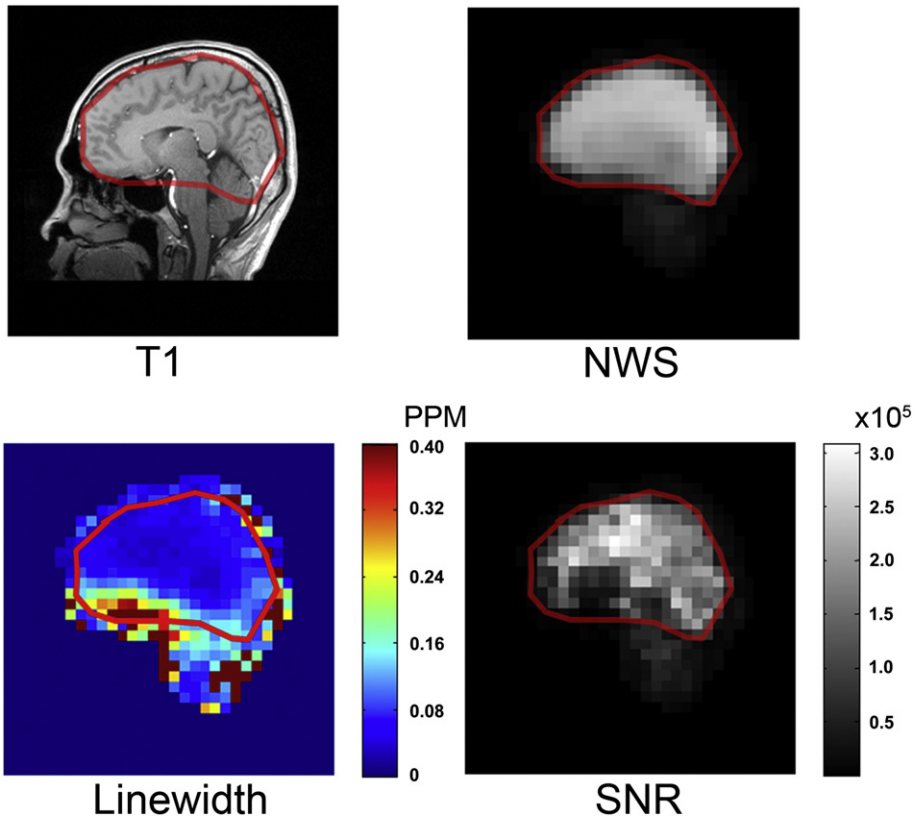

Fig. 2. Signal distribution and spectral quality of the non-water-suppressed (NWS) proton spectra from a representative subject. (Upper left) The anatomical (T1) reference image with the boundary of the NWS image (upper right) delineated in red. (Upper right) The NWS image was obtained by integration of the non-suppressed water peak (brighter color corresponds to higher intensity). Spectral quality was evaluated by the linewidth (lower left) and the SNR (lower right) of the water peak. The SNR was calculated as the ratio between the integrated water peak and the baseline noise.

posterior cingulate ROIs and the lowest concentrations were found in the mid cingulate and thalamic ROIs. The relationship was opposite for tCho (Table 2). Across all ROIs, TEavg resulted in higher NAA concentrations and lower tCr and tCho concentrations than TE30. TEavg also resulted in higher Glu concentrations in all ROIs but the occipital and thalamic, probably due to suboptimal CRLBs for the latter two (Table 2). To explore the effect of the two TE protocols on the positive relationship between NAA and Glu (Kaiser et al., 2005), correlations were performed between concentrations of NAA and Glx and Glu. For all ROIs but the occipital, a significant positive correlation between NAA and Glx was observed for TE30 ($N=16$, one-tailed, r-range: 0.457–0.672, P-range: 0.0022–0.038, occipital $r=0.367$, occipital $P=0.081$). For TEavg, only the ROIs in the entire medial wall ($r=0.498$, $P=0.025$), the anterior CC ($r=0.442$, $P=0.043$) and the thalamus ($r=0.628$, $P=0.005$) exhibited a significant positive relationship between NAA and Glu concentrations. Significant correlations were not observed for NAA and Glu using TE30 or for NAA and Glx using TEavg.

TE30 resulted in mean CRLBs below 7% for NAA, tCr and tCho in all ROIs (Table 2). Slightly higher mean CRLBs were found for mI (8.33%–13.82%). As predicted for TE30, the mean CRLB for Glx was substantially lower than for Glu and Gln separately. The mean CRLBs obtained with TEavg were similar to those from TE30 for tCr and tCho, slightly higher for NAA, and substantially higher for mI in all the ROIs. Compared with TE30, TEavg resulted in substantially lower mean CRLBs for Glu and substantially higher mean CRLBs for Gln and Glx in most of the ROIs indicating successful spectral editing of Glu (Table 2). Satisfactory CRLBs (<20 %) were not obtained for Glu in the occipital and the thalamic ROIs (Table 2). The decrease in Glu CRLB and the increase in Glx CRLB with TEavg were significant for all ROIs but the occipital and thalamic (Table 3). The majority of ROIs also survived an adjusted threshold.

Table 4 presents the short- (immediate within-day) and long-term (between-weeks) reproducibility of the two protocols as assessed by the COV in the 8 ROIs. In general, the COV decreased with increasing ROI size (number of voxels). The smallest COV was obtained with the ROI covering the entire cortex of the medial wall and the largest COV was obtained in the thalamic ROI. For TE30, the COVs improved substantially in most of the ROIs when quantifying Glu and Gln together

Table 1
Comparison of the spectral quality in 8 regions using a constant short-TE (TE30) and TE-averaging (TEavg).

Parameter	Protocol	MW	CC	Parietal	Occipital	Ant CC	Mid CC	Post CC	Tha
SNR	TE30	15.8 ± 1.6	16.5 ± 1.6	17.0 ± 1.9	17.6 ± 3.0	16.4 ± 2.3	17.5 ± 1.9	20.4 ± 2.2	12.5 ± 1.9
	TEavg	11.5 ± 1.2	12.6 ± 1.9	11.9 ± 2.0	11.8 ± 3.0	12.3 ± 2.6	13.6 ± 2.8	15.6 ± 2.2	8.9 ± 1.5
FWHM	TE30	0.083 ± 0.010	0.076 ± 0.013	0.088 ± 0.021	0.098 ± 0.026	0.069 ± 0.015	0.060 ± 0.009	0.065 ± 0.014	0.080 ± 0.015
	TEavg	0.080 ± 0.009	0.073 ± 0.010	0.087 ± 0.021	0.095 ± 0.022	0.069 ± 0.016	0.061 ± 0.010	0.066 ± 0.011	0.078 ± 0.012
SNR	P-value	<**0.001**	<**0.001**	<**0.001**	<**0.001**	<**0.001**	<**0.001**	<**0.001**	<**0.001**
FWHM	P-value	<**0.001**	0.033	0.7024	0.0929	0.8641	0.3821	0.2585	0.115

SNR, signal-to-noise ratio; FWHM, full width at half maximum, MW, medial wall; CC, cingulate cortex; Ant, anterior; Post, posterior; Tha, thalamus; TE, echo time. Values in bold passed a Bonferroni correction (8 regions).

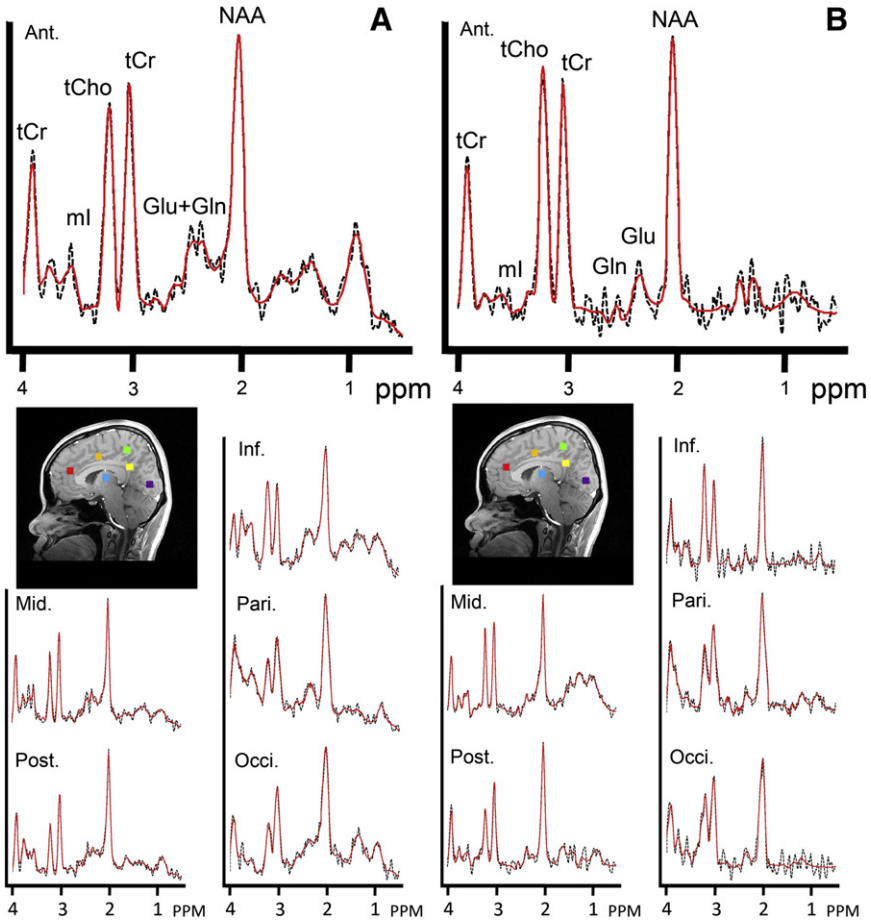

Fig. 3. Spectra (black) with overlaid LCModel fit (red) from a single voxel at 6 locations in a representative subject. Spectra were obtained with (A) a constant short-TE (TE30) and (B) TE-averaging (TEavg). Metabolite peaks are labeled in the upper 2 spectra and the 6 voxel locations are marked on the anatomical image: Ant, anterior cingulate (red); Mid, mid cingulate (orange); Post, posterior cingulate (yellow); Inf, inferior (thalamus) (blue); Pari, medial parietal cortex (green); and Occi, medial occipital cortex (purple).Note the emergence of the glutamate peak around 2.35 ppm, the reduction in the myo-inositol peak around 3.5 ppm, and the flattening of the baseline in the TEavg spectra. PPM denotes parts per million.

(Glx) compared to separately. Short-term reproducibility resulting from TEavg differed with respect to TE30. For the metabolites tCr and tCho, COVs were either similar or slightly better for all ROIs using TEavg. The COVs for NAA, mI, Gln, and Glx were substantially worse for most ROIs using TEavg. Mixed results were obtained for Glu. Comparing long-term reproducibility obtained with the two TE protocols, TEavg resulted in similar or lower COVs for tCr and Glu and higher COVs for NAA, tCho, mI, Gln, and Glx. Finally, for both TE protocols the long-term paradigm mostly resulted in increased variability/decreased reproducibility relative to the short-term paradigm.

Discussion

In the present study, phased-array detection at 3 T was used to acquire sagittal PEPSI data from the right medial wall of the cortex with a relatively fine spatial resolution. Data acquisitions were within a clinically acceptable scan time that is potentially less confounded by head motion. Absolute metabolite concentrations were quantified by means of an automatic procedure and by using tissue water as a concentration reference. An internal reference is preferable to an external reference unless changes in tissue water content are expected (Minati et al., 2010). Short- and long-term reproducibility was assessed in multiple ROIs using a constant short-TE protocol and a TE-averaged protocol. These protocols were employed due to the additional information they provide about Glu. ROIs consisted of voxel clusters rather than single voxels since these are less influenced by repositioning accuracy (Li et al., 2002).

The TE protocols

One of the main findings of this study was a substantially better spectral quality and similar or lower quantitation uncertainty for all metabolites (CRLB<20%), except Glu, using TE30. As expected, the TE30 protocol resulted in reduced quantitation uncertainty and increased reproducibility when Glu and Gln were quantified together (Glx) rather than separately. This is mainly due to the still existing spectral overlap of the C4 multiplet proton resonances of Glu and Gln at 2.35 ppm and 2.45 ppm, respectively (Yang et al., 2008). TEavg resulted in higher Glu concentrations and lowered Glu quantitation uncertainty bringing Glu within a satisfactory level (CRLB<20%). However, TEavg did not result in a systematically improved short- or long-term reproducibility for Glu or any other metabolites. This is despite TE averaging results in a simplified spectrum with fewer resonance overlaps and flattening of the baseline due to suppression of macromolecular and lipid resonances.

Fig. 4. Interpolated metabolite concentration maps (in I.U.) from the right medial wall and the matched uninterpolated CRLB maps (in percent) from the first scans for a representative subject. Maps are shown for the two protocols using (A) a constant short-TE (TE30) and (B) TE-averaging (TEavg). Voxels are shown within the "medial-wall" mask. Note the different color scales for different metabolites.

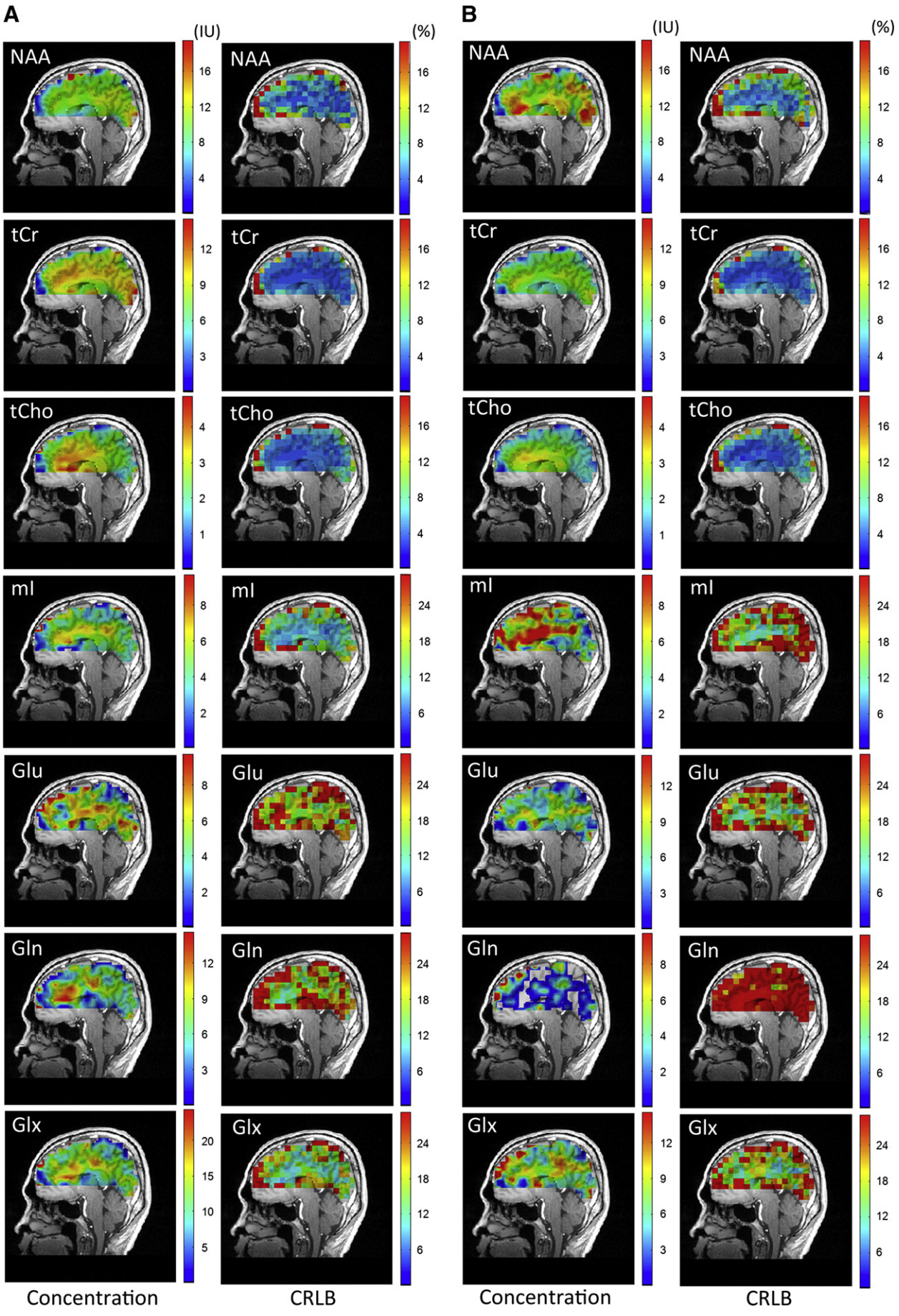
A
B
(IU)
(%)
NAA
tCr
tCho
mI
Glu
Gln
Glx
Concentration
CRLB

Our finding is in agreement with previous experimental observations and emphasizes that reduced quantitation uncertainty may not necessarily improve the reproducibility (Langer et al., 2007). Taken together, the summation over multiple TEs provided improved and reliable Glu quantification without interference from overlapping metabolites. This came at the cost of less reliable quantification of several metabolites including NAA, mI and Gln which may provide additional important clinical information. Additionally, the known positive relationship between NAA and Glu concentrations could not be consistently confirmed using TEavg (Kaiser et al., 2005). It is noteworthy to mention that although absolute quantitation of short-TE spectra benefits from incorporation of a priori information about macromolecular and lipid contributions (Gottschalk et al., 2008; Kanowski et al., 2004; Seeger et al., 2003), the increased complexity of the TE30 spectra likely results in slightly reduced accuracy compared to TEavg. Also, better results may be obtained with TEavg with better shimming conditions, e.g. with acquisition in the transverse plane.

Regional variation

Spectral assessment was performed in neuroanatomical loci throughout the medial wall and in ROIs with different spatial extend. For both TE protocols, regional variation in spectral quality was observed among the 4 smallest same-sized ROIs. The thalamic ROI exhibited the lowest SNR and the widest linewidth and the posterior CC ROI exhibited the highest SNR but similar linewidth as the other cingulate ROIs. The thalamic ROI also exhibited the lowest concentrations and the highest quantitation uncertainty for all metabolites but tCho. The opposite was the case for the posterior CC ROI which in general exhibited high concentrations and low quantitation uncertainty except for tCho. The relatively poorer spectral quality in the thalamus likely explains why TEavg did not yield a satisfactory result for Glu in this ROI.

The regional concentration profiles may be related to the density of the cellular matrix and the metabolic demand in the sampled volume. NAA is predominantly produced in neurons and tCho is often considered a marker of membrane turnover and density, including myelination (Soares and Law, 2009). Glu is mainly found within neurons (Ottersen et al., 1992; Patel et al., 1982), its concentration correlates with that of NAA (Kaiser et al., 2005) and it is tightly linked to glucose metabolism (Hertz, 2004). The high levels of NAA and Glu (Glx) and low levels of tCho in the posterior CC may represent a relatively higher grey matter density and/or metabolic demand. In support of this, the posterior CC has the highest glucose metabolism in the human brain (Minoshima et al., 1997), a high regional blood flow (Andreasen et al., 1995; Raichle et al., 2001), as well as a high cytochrome oxidase activity indicative of mitochondrial density and energy consumption (Vogt and Laureys, 2005). The highest tCho concentration was found in the thalamus but with similar quantitation uncertainty as the other same-sized ROIs. Relatively high levels of thalamic tCho or Cho/Cre have previously been reported, using different techniques and parameters (Geurts et al., 2006; Tedeschi et al., 1996). A lower absolute Cho concentration in the thalamus than in the anterior CC has also been reported (Yoo et al., 2009). It is conceivable that the high levels of tCho may reflect a white matter contribution from the fornix to the ROI composition (and from the corpus callosum for the anterior CC). However, thalamus is also targeted by dense cholinergic projections from the midbrain and contains the highest density of nicotinic acetyl choline receptors in the brain (Kuwabara et al., 2012). Thus, a contribution from the neurotransmitter acetyl choline cannot be ruled out.

Reproducibility

Regional reproducibility was addressed to establish the magnitude of metabolic changes to be considered significant using short- and long-term repetitive measurements. The TE-averaged protocol was implemented to specifically assess the reproducibility of Glu. For both short- and long-term repetitions, pairwise comparison of Glu concentrations using TEavg requires a difference of 5–8% for the large ROIs, 12–17% for the medium sized ROIs and 16–26% for the smaller cingulate ROIs. The variations obtained by TE30 for the less specific Glx were 3–5%, 8–10% and 10–15%. This finding is not surprising as Glx measured with TE30 results in better SNRs than the more specific Glu measured with TEavg. Hence, the cost of more specific metabolic information is the requirement of an increased effect size especially with increasing anatomical specificity. This comes in addition to the loss of sensitivity for other metabolites. For the three dominating metabolites in the spectrum, NAA, tCr and tCho, variations associated with long-term repetition using TE30 were between 2 and 10%. Direct comparison with other studies is made difficult by differences in the methodology, i.e. field strength, slice orientation, NEX, TE and TR durations, number of subjects, and the level of analysis (single voxels or larger ROIs). A recent study using phased-array detection at 3 T for 3D MRSI acquisition found COVs for NAA, Cr and Cho in lobar regions and the entire cerebrum ranging between 3 and 6.5% (Maudsley et al., 2010). Other MRSI studies using the same constant short-TE as in this study, but with a less robust voxel-based analysis, found COVs ranging between 10–22% and 16–24% for the three major metabolites and Glx, respectively (Chard et al., 2002; Langer et al., 2007). Another study using the same NEX and TR as in this study, but with long TE and at 1.5 T, found lobar COVs in the range 3–13% and 2–7% for NAA/Cr and Cho/Cr, respectively (Gu et al., 2008). Overall, our reproducibility results compares favorably with these findings, especially when considering the volume of the lobar regions or the cerebrum.

Methodological considerations

The reproducibility investigated in this study primarily reflects variations in instrumental factors and spectral quality. Due to the relatively short time intervals between scans, biological variations can be assumed to be negligible. In agreement with previous results (Chard et al., 2002; Gu et al., 2008; Li et al., 2002; Maudsley et al., 2010; Tedeschi et al., 1996), we found the reproducibility to depend on the specific metabolite, the size of the sampled volume (cf. CC ROI versus same-sized cingulate ROIs) as well as on the anatomical location (cf. same-sized ROIs). Considering the influence of spectral quality on reproducibility, a systematic effect was not found among the same sized ROIs in the cingulate although a substantially higher SNR was obtained in the posterior CC. For the majority of the ROIs, greater sensitivity was obtained by integrating results over a larger volume. However, the higher COVs found in the thalamus may be attributed to factors influencing the spectral quality such as partial volume effects (proximity to the ventricles and the fornix) and field inhomogeneity. The COVs from the occipital ROI tended to be of similar magnitude as those from the smaller cingulate ROIs. The larger spectral linewidth observed for the occipital ROI, possibly caused by lipid saturation due to the proximity to outer regions, may explain this finding. For immediate repetitions, Glx (TE30) and Glu (TEavg) reproducibility in the posterior CC was of the same magnitude as from the substantially larger parietal ROI. This was not the case for long-term repetitions indicating that larger volumes provide more robust glutamatergic information in longitudinal follow-up paradigms or that immediate repetitions allow for smaller sample volumes. This is in agreement with larger ROIs being less dependent on methodological factors such as head movement and repositioning accuracy (Li et al., 2002). The latter may contribute more in longitudinal follow-up paradigms. Apart from optimization of post acquisition localization and volume of ROIs, improvements in reproducibility may, to some extent, also be obtained by increasing the number of excitations. However, this would increase the scan time.

Table 2
Metabolite concentrations (CONC) and the corresponding Cramer–Rao lower bound (CRLB) for 8 regions of interest using a constant short-TE (TE30) and TE averaging (TEavg).

		MW	CC	Parietal	Occipital	Ant CC	Mid CC	Post CC	Tha
TE30									
NAA	CONC	11.22 ± 0.95	11.64 ± 0.96	12.28 ± 1.63	13.96 ± 1.11	11.85 ± 1.10	11.26 ± 1.20	13.03 ± 1.08	10.08 ± 1.21
	CRLB	5.38 ± 0.46	4.87 ± 0.60	4.39 ± 0.89	4.47 ± 0.88	4.44 ± 0.84	4.83 ± 1.16	3.50 ± 0.62	5.39 ± 1.28
tCr	CONC	9.43 ± 0.72	9.95 ± 0.71	10.18 ± 1.06	11.38 ± 1.48	10.46 ± 1.36	9.46 ± 0.75	10.45 ± 1.04	9.66 ± 1.42
	CRLB	4.57 ± 0.26	3.88 ± 0.31	4.06 ± 0.42	3.99 ± 0.59	3.70 ± 0.54	3.52 ± 0.32	3.23 ± 0.23	4.27 ± 0.56
tCho	CONC	2.55 ± 0.32	2.63 ± 0.35	2.33 ± 0.40	2.06 ± 0.45	2.94 ± 0.47	2.62 ± 0.43	2.35 ± 0.33	3.21 ± 0.50
	CRLB	5.72 ± 0.49	4.81 ± 0.48	5.72 ± 0.60	6.73 ± 1.03	4.33 ± 0.66	4.34 ± 0.64	4.38 ± 0.58	4.31 ± 0.66
mI	CONC	5.08 ± 0.52	5.32 ± 0.62	4.93 ± 0.83	4.64 ± 0.82	5.52 ± 0.95	5.54 ± 1.22	6.21 ± 1.31	4.59 ± 0.94
	CRLB	12.61 ± 0.85	10.94 ± 1.01	12.08 ± 2.25	13.16 ± 3.35	10.78 ± 2.85	10.22 ± 3.79	8.33 ± 1.62	13.82 ± 3.83
Glu	CONC	6.06 ± 0.39	5.80 ± 0.38	5.54 ± 0.94	6.76 ± 0.76	6.28 ± 1.67	5.68 ± 1.22	6.16 ± 1.11	6.05 ± 1.75
	CRLB	22.25 ± 1.62	22.54 ± 2.28	23.36 ± 4.18	19.46 ± 2.52	22.14 ± 6.66	22.97 ± 5.66	19.72 ± 4.82	21.55 ± 6.34
Gln	CONC	8.58 ± 0.66	9.03 ± 1.00	8.33 ± 1.36	9.10 ± 1.43	9.35 ± 1.85	8.96 ± 2.07	9.54 ± 2.45	5.83 ± 1.77
	CRLB	18.93 ± 2.17	17.30 ± 2.72	18.27 ± 3.47	17.15 ± 4.27	17.77 ± 5.42	16.83 ± 3.12	16.48 ± 4.69	26.03 ± 7.35
Glx	CONC	13.02 ± 0.83	14.03 ± 1.24	12.97 ± 1.48	15.21 ± 1.58	15.07 ± 2.45	14.39 ± 2.59	15.34 ± 2.54	10.12 ± 2.19
	CRLB	15.37 ± 1.56	13.53 ± 1.96	14.03 ± 1.79	11.96 ± 2.53	12.94 ± 3.21	12.66 ± 2.04	12.37 ± 2.80	17.86 ± 5.36
TEavg									
NAA	CONC	12.47 ± 1.16	12.33 ± 1.21	13.49 ± 2.46	15.70 ± 2.16	12.47 ± 1.38	11.47 ± 1.85	14.34 ± 2.98	11.76 ± 3.08
	CRLB	7.34 ± 0.66	6.36 ± 1.01	7.42 ± 1.15	7.96 ± 2.04	5.76 ± 1.03	5.70 ± 1.82	5.35 ± 1.30	8.30 ± 2.02
tCr	CONC	6.96 ± 0.50	7.37 ± 0.48	7.70 ± 0.90	8.16 ± 0.76	7.86 ± 0.81	7.02 ± 0.60	8.18 ± 0.62	7.07 ± 1.06
	CRLB	4.83 ± 0.43	3.93 ± 0.39	4.11 ± 0.45	4.30 ± 0.91	3.52 ± 0.43	3.50 ± 0.49	3.22 ± 0.35	4.61 ± 0.93
tCho	CONC	2.03 ± 0.24	2.11 ± 0.25	1.87 ± 0.29	1.56 ± 0.26	2.42 ± 0.41	2.13 ± 0.27	1.94 ± 0.26	2.60 ± 0.43
	CRLB	5.96 ± 0.46	4.92 ± 0.47	5.73 ± 0.52	7.26 ± 1.54	4.36 ± 0.61	4.25 ± 0.63	4.56 ± 0.36	4.64 ± 0.81
mI	CONC	7.27 ± 0.49	7.36 ± 0.45	6.09 ± 0.94	7.34 ± 1.62	8.19 ± 1.31	8.07 ± 1.65	7.16 ± 1.68	7.16 ± 1.99
	CRLB	19.05 ± 1.34	17.20 ± 1.90	21.25 ± 4.15	20.48 ± 4.38	15.30 ± 3.28	14.51 ± 4.72	16.39 ± 5.94	20.57 ± 5.69
Glu	CONC	7.17 ± 0.40	7.38 ± 0.53	7.00 ± 1.55	6.41 ± 1.08	7.98 ± 1.73	6.79 ± 1.55	7.68 ± 1.81	5.09 ± 1.56
	CRLB	19.22 ± 1.81	16.96 ± 2.10	19.44 ± 6.17	23.50 ± 5.13	15.97 ± 4.44	16.25 ± 4.47	15.54 ± 4.60	30.55 ± 8.70
Gln	CONC	5.73 ± 1.68	4.67 ± 0.98	4.24 ± 1.01	6.61 ± 3.28	5.29 ± 1.86	4.29 ± 2.28	4.34 ± 0.92	N/A
	CRLB	29.06 ± 3.21	29.21 ± 5.34	30.27 ± 3.76	29.40 ± 7.65	28.50 ± 14.39	31.74 ± 11.78	26.13 ± 3.07	N/A
Glx	CONC	8.72 ± 0.51	9.04 ± 0.73	8.21 ± 1.56	8.53 ± 1.29	9.55 ± 2.02	8.46 ± 2.08	9.17 ± 2.06	6.51 ± 2.01
	CRLB	18.76 ± 1.71	16.37 ± 2.11	19.16 ± 5.42	20.64 ± 3.25	15.76 ± 4.05	16.09 ± 4.93	14.99 ± 3.58	25.96 ± 8.89

NAA, N-acetyl aspartate; tCr, total creatine; tCho, total choline; mI, myo-inositol ; Glu, glutamate; Gln, glutamine; Glx, glutamate and glutamine; N/A, not available
Note: concentrations are given in institutional units. Values are taken from the first sessions and are given as mean± standard deviation. See Table 1 for further details.

Sagittal PEPSI acquisition is advantageous for assessing metabolite distributions in the medial wall of the brain with one slice. However, data acquisition in this plane also offers some disadvantages compared to acquisition in the transverse plane. Sagittal echo-planar imaging is known to be more susceptible to field inhomogeneities in the orbitofrontal and subcortical areas. This leads to degraded spectral quality and poor metabolite quantification. Furthermore, spatial distortions in these regions can potentially cause ROI mis-localizations. In the present study, mis-localization effects were minimized by acquiring the T1 images at the same spatial location and with the same FOV as the PEPSI data. Both T1 and PEPSI data were acquired with the same readout direction, i.e. anterior–posterior direction, but with different readout bandwidth. The latter may lead to minor mis-localization errors, especially in the thalamic ROI.

Although PEPSI profits from better spatial coverage compared to chemical shift imaging (CSI) and single voxel acquisitions, this also renders the method increasingly sensitive to field inhomogeneities resulting in degraded spectral quality in the affected brain regions. It is therefore necessary to optimize the shimming volume to the region of interest. In addition, lipid contamination is a major confound in outer regions such as the cortex. Placement and optimization of the thickness of the outer-volume lipid suppression bands is time-consuming and require skill and experience to adequately suppress peripheral lipid areas while minimizing suppression of cortical regions. Moreover, PEPSI at short TEs may lead to line-shape distortion, due to eddy currents from time varying gradients. However, the particular sequence used in this study has been shown to have similar sensitivity and linewidth as CSI (Otazo et al., 2006). It remains to be seen if the results reported here specifically apply to phased array coils or if they can be replicated by other types of coils. Our data suggest that the results are influenced relatively little by the different depth sensitivity of phased array coils, probably because the ROIs were placed in proximity to the central part of the coil.

Conclusions

The present study established the variability of metabolites in the medial wall of the cortex for immediate and long-term repetition of measurements. Based on this, it is possible to set the magnitude of metabolic change to be considered significant in the context of biological variability. Reproducibility was found to depend on the specific metabolite, the size of the sampled volume as well as on the anatomical location. The protocols achieved relatively low COVs with TE30 mostly showing better sensitivity than TEavg. However, while TEavg enhanced Glu and suppressed Gln, TE30 did not resolve the two metabolites. The cost of more specific glutamatergic information (Glu versus Glx) is the requirement of an increased effect size especially with increasing anatomical

Table 3
Comparison of Glu and Glx CRLBs between the TE30 and TEavg protocols in 8 regions.

Metabolite		MW	CC	Parietal	Occipital	Ant CC	Mid CC	Post CC	Tha
P-values	Glu	<**0.001**	<**0.001**	0.0140	0.9964	**0.0030**	**0.0028**	0.0147	0.9936
	Glx	<**0.001**	<**0.001**	**0.0012**	<**0.001**	0.0092	0.0125	**0.0050**	0.0078

Note, P-values were obtained from a paired one-tailed t-test between TE30 and TEavg. Data from the first session was used. Values in bold passed a Bonferroni correction (8 regions). See other Tables for further details.

Table 4
Short- (within-day) and long-term (between-weeks) reproducibility of the two TE protocols as assessed by the COV in 8 regions-of-interest.

Within-day								
TE30	MW	CC	Parietal	Occipital	Ant CC	Mid CC	Post CC	Tha
NAA	1.2%	1.4%	2.7%	3.8%	3.9%	5.2%	3.9%	5.0%
tCr	1.5%	2.0%	4.3%	4.0%	4.9%	4.1%	4.2%	4.7%
tCho	2.5%	2.5%	3.9%	6.6%	6.0%	5.1%	6.2%	8.4%
mI	2.5%	4.0%	7.5%	13.0%	11.2%	9.8%	9.5%	14.3%
Glu	5.1%	7.3%	10.8%	11.9%	25.4%	20.8%	13.3%	32.6%
Gln	3.5%	5.1%	9.5%	9.6%	19.5%	13.3%	13.0%	33.7%
Glx	2.5%	4.4%	9.7%	9.8%	13.9%	11.3%	9.8%	17.3%
TEavg								
NAA	2.6%	4.1%	5.4%	8.1%	13.6%	13.1%	12.7%	8.9%
tCr	1.8%	2.2%	3.1%	3.9%	3.0%	4.6%	4.6%	6.8%
tCho	2.3%	2.4%	3.1%	4.7%	3.6%	4.2%	3.4%	6.9%
mI	5.1%	9.7%	17.7%	20.9%	21.8%	25.1%	20.3%	26.4%
Glu	5.2%	7.3%	15.6%	16.6%	16.6%	18.9%	16.7%	26.4%
Gln	13.7%	19.1%	20.9%	27.8%	42.3%	38.0%	23.3%	N/A
Glx	5.8%	8.3%	9.8%	10.9%	9.7%	27.3%	12.8%	28.2%
Between-weeks								
NAA	1.7%	2.9%	7.2%	4.2%	5.7%	1.9%	3.9%	7.3%
tCr	2.3%	2.6%	5.9%	4.1%	9.7%	3.8%	3.6%	10.0%
tCho	2.1%	3.6%	9.7%	8.9%	7.6%	5.7%	2.9%	7.4%
mI	2.6%	4.9%	17.0%	4.8%	13.6%	15.6%	15.6%	11.8%
Glu	3.8%	7.7%	17.0%	13.9%	25.4%	19.6%	21.3%	24.2%
Gln	3.2%	6.8%	10.5%	8.9%	14.4%	20.0%	19.7%	27.2%
Glx	3.5%	3.7%	9.9%	7.8%	14.5%	14.0%	15.0%	22.1%
TEavg								
NAA	2.9%	3.9%	10.5%	4.0%	13.8%	7.8%	13.0%	13.8%
tCr	2.1%	3.0%	6.1%	7.3%	7.8%	4.4%	3.0%	7.5%
tCho	4.2%	5.1%	6.7%	10.5%	11.5%	7.6%	8.8%	9.9%
mI	5.3%	8.7%	8.0%	17.6%	21.9%	9.6%	17.1%	26.4%
Glu	5.4%	6.1%	11.7%	14.3%	25.9%	15.6%	21.4%	16.8%
Gln	19.2%	22.0%	32.6%	N/A	N/A	53.1%	30.4%	N/A
Glx	4.6%	5.9%	13.4%	10.3%	28.2%	14.8%	23.8%	14.7%

COV, coefficient of variation. See Table 1 for further details.

specificity. The protocols implemented here are reliable and may be used to study disease progression and intervention mechanisms.

Acknowledgments

This study was supported by grants from the National Science Council (99-2314-B-010-010-MY3 and 100-2320-B-004-002) and the "Aim for the top university plan from Ministry of Education for National Yang-Ming University". Data was acquired at National Yang-Ming University.

References

Andreasen, N.C., O'Leary, D.S., Cizadlo, T., Arndt, S., Rezai, K., Watkins, G.L., Ponto, L.L., Hichwa, R.D., 1995. Remembering the past: two facets of episodic memory explored with positron emission tomography. Am. J. Psychiatry 152, 1576–1585.

Apkarian, A.V., Hashmi, J.A., Baliki, M.N., 2011. Pain and the brain: specificity and plasticity of the brain in clinical chronic pain. Pain 152, S49–S64 (Epub 2010 Dec 2013).

Beck, A.T., Ward, C.H., Mendelson, M., Mock, J., Erbaugh, J., 1961. An inventory for measuring depression. Arch. Gen. Psychiatry 4, 561–571.

Bennett, M.R., 2011. The prefrontal-limbic network in depression: modulation by hypothalamus, basal ganglia and midbrain. Progress 93, 468–487 (Epub 2011 Feb 2022).

Chard, D.T., McLean, M.A., Parker, G.J., MacManus, D.G., Miller, D.H., 2002. Reproducibility of in vivo metabolite quantification with proton magnetic resonance spectroscopic imaging. J. Magn. Reson. Imaging 15, 219–225.

Gasparovic, C., Song, T., Devier, D., Bockholt, H.J., Caprihan, A., Mullins, P.G., Posse, S., Jung, R.E., Morrison, L.A., 2006. Use of tissue water as a concentration reference for proton spectroscopic imaging. Magn. Reson. Med. 55, 1219–1226.

Geurts, J.J., Reuling, I.E., Vrenken, H., Uitdehaag, B.M., Polman, C.H., Castelijns, J.A., Barkhof, F., Pouwels, P.J., 2006. MR spectroscopic evidence for thalamic and hippocampal, but not cortical, damage in multiple sclerosis. Magn. Reson. Med. 55, 478–483.

Gonenc, A., Govind, V., Sheriff, S., Maudsley, A.A., 2010. Comparison of spectral fitting methods for overlapping J-coupled metabolite resonances. Magnetic 64, 623–628.

Gottschalk, M., Lamalle, L., Segebarth, C., 2008. Short-TE localised 1H MRS of the human brain at 3 T: quantification of the metabolite signals using two approaches to account for macromolecular signal contributions. NMR Biomed. 21, 507–517.

Gu, M., Kim, D.H., Mayer, D., Sullivan, E.V., Pfefferbaum, A., Spielman, D.M., 2008. Reproducibility study of whole-brain 1H spectroscopic imaging with automated quantification. Magn. Reson. Med. 60, 542–547.

Harris, R.E., Sundgren, P.C., Pang, Y., Hsu, M., Petrou, M., Kim, S.H., McLean, S.A., Gracely, R.H., Clauw, D.J., 2008. Dynamic levels of glutamate within the insula are associated with improvements in multiple pain domains in fibromyalgia. Arthritis Rheum. 58, 903–907.

Hertz, L., 2004. Intercellular metabolic compartmentation in the brain: past, present and future. Neurochem. Int. 45, 285–296.

Hurd, R., Sailasuta, N., Srinivasan, R., Vigneron, D.B., Pelletier, D., Nelson, S.J., 2004. Measurement of brain glutamate using TE-averaged PRESS at 3T. Magn. Reson. Med. 51, 435–440.

Kaiser, L.G., Schuff, N., Cashdollar, N., Weiner, M.W., 2005. Age-related glutamate and glutamine concentration changes in normal human brain: 1H MR spectroscopy study at 4 T. Neurobiol. Aging 26, 665–672.

Kanowski, M., Kaufmann, J., Braun, J., Bernarding, J., Tempelmann, C., 2004. Quantitation of simulated short echo time 1H human brain spectra by LCModel and AMARES. Magn. Reson. Med. 51, 904–912.

Kuwabara, H., Wong, D.F., Gao, Y., Valentine, H., Holt, D.P., Ravert, H.T., Dannals, R.F., Horti, A.G., 2012. PET imaging of nicotinic acetylcholine receptors in baboons with 18F-AZAN, a radioligand with improved brain kinetics. J. Nucl. Med. 53, 121–129 (Epub 2011 Dec 2015).

Langer, D.L., Rakaric, P., Kirilova, A., Jaffray, D.A., Damyanovich, A.Z., 2007. Assessment of metabolite quantitation reproducibility in serial 3D-(1)H-MR spectroscopic imaging of human brain using stereotactic repositioning. Magn. Reson. Med. 58, 666–673.

Li, B.S., Babb, J.S., Soher, B.J., Maudsley, A.A., Gonen, O., 2002. Reproducibility of 3D proton spectroscopy in the human brain. Magn. Reson. Med. 47, 439–446.

Lin, F.H., Tsai, S.Y., Otazo, R., Caprihan, A., Wald, L.L., Belliveau, J.W., Posse, S., 2007. Sensitivity-encoded (SENSE) proton echo-planar spectroscopic imaging (PEPSI) in the human brain. Magn. Reson. Med. 57, 249–257.

Mangia, S., Tkac, I., Logothetis, N.K., Gruetter, R., Van de Moortele, P.F., Ugurbil, K., 2007. Dynamics of lactate concentration and blood oxygen level-dependent effect in the human visual cortex during repeated identical stimuli. J. Neurosci. Res. 85, 3340–3346.

Maudsley, A.A., Domenig, C., Sheriff, S., 2010. Reproducibility of serial whole-brain MR spectroscopic imaging. NMR 23, 251–256.

Minati, L., Aquino, D., Bruzzone, M.G., Erbetta, A., 2010. Quantitation of normal metabolite concentrations in six brain regions by in-vivo H-MR spectroscopy. J. Med. Phys. 35, 154–163.

Minoshima, S., Giordani, B., Berent, S., Frey, K.A., Foster, N.L., Kuhl, D.E., 1997. Metabolic reduction in the posterior cingulate cortex in very early Alzheimer's disease. Ann. Neurol. 42, 85–94.

Mullins, P.G., Rowland, L.M., Jung, R.E., Sibbitt Jr., W.L., 2005. A novel technique to study the brain's response to pain: proton magnetic resonance spectroscopy. NeuroImage 26, 642–646.

Mullins, P.G., Chen, H., Xu, J., Caprihan, A., Gasparovic, C., 2008. Comparative reliability of proton spectroscopy techniques designed to improve detection of J-coupled metabolites. Magn. Reson. Med. 60, 964–969.

Otazo, R., Mueller, B., Ugurbil, K., Wald, L., Posse, S., 2006. Signal-to-noise ratio and spectral linewidth improvements between 1.5 and 7 Tesla in proton echo-planar spectroscopic imaging. Magn. Reson. Med. 56, 1200–1210.

Ottersen, O.P., Zhang, N., Walberg, F., 1992. Metabolic compartmentation of glutamate and glutamine: morphological evidence obtained by quantitative immunocytochemistry in rat cerebellum. Neuroscience 46, 519–534.

Pan, J.W., Williamson, A., Cavus, I., Hetherington, H.P., Zaveri, H., Petroff, O.A., Spencer, D.D., 2008. Neurometabolism in human epilepsy. Epilepsia 49, 31–41.

Patel, A.J., Hunt, A., Gordon, R.D., Balazs, R., 1982. The activities in different neural cell types of certain enzymes associated with the metabolic compartmentation glutamate. Brain Res. 256, 3–11.

Petroff, O.A., Errante, L.D., Rothman, D.L., Kim, J.H., Spencer, D.D., 2002. Glutamate–glutamine cycling in the epileptic human hippocampus. Epilepsia 43, 703–710.

Provencher, S.W., 1993. Estimation of metabolite concentrations from localized in vivo proton NMR spectra. Magn. Reson. Med. 30, 672–679.

Raichle, M.E., MacLeod, A.M., Snyder, A.Z., Powers, W.J., Gusnard, D.A., Shulman, G.L., 2001. A default mode of brain function. Proc. Natl. Acad. Sci. U. S. A. 98, 676–682.

Seeger, U., Klose, U., Mader, I., Grodd, W., Nagele, T., 2003. Parameterized evaluation of macromolecules and lipids in proton MR spectroscopy of brain diseases. Magn. Reson. Med. 49, 19–28.

Soares, D.P., Law, M., 2009. Magnetic resonance spectroscopy of the brain: review of metabolites and clinical applications. Clin. Radiol. 64, 12–21 (Epub 2008 Aug 2030).

Soher, B.J., Young, K., Bernstein, A., Aygula, Z., Maudsley, A.A., 2007. GAVA: spectral simulation for in vivo MRS applications. J. Magn. Reson. 185, 291–299 (Epub 2007 Jan 2012).

Srinivasan, R., Sailasuta, N., Hurd, R., Nelson, S., Pelletier, D., 2005. Evidence of elevated glutamate in multiple sclerosis using magnetic resonance spectroscopy at 3 T. Brain 128, 1016–1025 (Electronic publication ahead of print 2005 Mar 1019).

Srinivasan, R., Cunningham, C., Chen, A., Vigneron, D., Hurd, R., Nelson, S., Pelletier, D., 2006. TE-averaged two-dimensional proton spectroscopic imaging of glutamate at 3 T. NeuroImage 30, 1171–1178 (Epub 2006 Jan 1123).

Tedeschi, G., Bertolino, A., Campbell, G., Barnett, A.S., Duyn, J.H., Jacob, P.K., Moonen, C.T., Alger, J.R., Di Chiro, G., 1996. Reproducibility of proton MR spectroscopic imaging findings. AJNR Am. J. Neuroradiol. 17, 1871–1879.

Tsai, S.Y., Posse, S., Lin, Y.R., Ko, C.W., Otazo, R., Chung, H.W., Lin, F.H., 2007. Fast mapping of the T2 relaxation time of cerebral metabolites using proton echo-planar spectroscopic imaging (PEPSI). Magn. Reson. Med. 57, 859–865.

Tsai, S.Y., Otazo, R., Posse, S., Lin, Y.R., Chung, H.W., Wald, L.L., Wiggins, G.C., Lin, F.H., 2008. Accelerated proton echo planar spectroscopic imaging (PEPSI) using GRAPPA with a 32-channel phased-array coil. Magn. Reson. Med. 59, 989–998.

Vogt, B.A., Laureys, S., 2005. Posterior cingulate, precuneal and retrosplenial cortices: cytology and components of the neural network correlates of consciousness. Prog Brain Res. 150, 205–217.

Yang, S., Hu, J., Kou, Z., Yang, Y., 2008. Spectral simplification for resolved glutamate and glutamine measurement using a standard STEAM sequence with optimized timing parameters at 3, 4, 4.7, 7, and 9.4T. Magn. Reson. Med. 59, 236–244.

Yoo, S.Y., Yeon, S., Choi, C.H., Kang, D.H., Lee, J.M., Shin, N.Y., Jung, W.H., Choi, J.S., Jang, D.P., Kwon, J.S., 2009. Proton magnetic resonance spectroscopy in subjects with high genetic risk of schizophrenia: investigation of anterior cingulate, dorsolateral prefrontal cortex and thalamus. Schizophr. Res. 111, 86–93 (Epub 2009 Apr 2029).